Influence of flame-generated vorticity on reaction-zone-surface area in weakly turbulent flows

INFLUENCE OF FLAME-GENERATED VORTICITY ON REACTION-ZONE-SURFACE AREA IN WEAKLY TURBULENT FLOWS

A.N. Lipatnikov*, V.A. Sabelnikov, S. Nishiki*** and T. Hasegawa******
lipatn@chalmers.se
*Chalmers University of Technology, Gothenburg, 41296, Sweden
**ONERA - The French Aerospace Lab., F-91761 Palaiseau, France
***Kagoshima University, Kagoshima 890-0065, Japan
****Nagoya University, Nagoya 464-8603, Japan

Abstract
Direct Numerical Simulation (DNS) data obtained from two statistically stationary, 1D, planar, weakly turbulent premixed flames are analyzed in order to examine the influence of flame-generated vorticity on the area of the reaction surface. The two flames are associated with the flamelet combustion regime and are characterized by significantly different density ratios, i.e. $\sigma = 7.53$ and 2.5, with all other things being roughly equal. Results indicate that generation of vorticity due to baroclinic torque within flamelets can impede wrinkling the reaction surface, reduce its area, and, hence, decrease burning rate. Thus, these results call for revisiting the widely-accepted concept of combustion acceleration due to flame-generated turbulence. In particular, in the case of $\sigma = 7.53$, the local stretch rate, which quantifies the local rate of an increase or decrease in the surface area, is predominantly negative in regions characterized by a large magnitude of enstrophy or a large magnitude of baroclinic torque term in the transport equation for the enstrophy, with the effect being more pronounced at larger values of the mean combustion progress variable. If $\sigma = 2.5$, baroclinic torque weakly effects vorticity field within the mean flame brush and the aforementioned effect is not pronounced.

Introduction
Almost seven decades ago, Karlovitz et al. [1] and Scurlock and Grover [2] put forward a seminal concept of combustion acceleration due to flame-generated turbulence in order to explain unexpectedly high burning rates obtained in some early experiments. For that purpose, they (i) highlighted two different (in the two different papers cited above) physical mechanisms of turbulence generation due to combustion-induced thermal expansion and (ii) hypothesized that such a flame-generated turbulence significantly increased the flame speed S_T, with the influence of the flame-generated turbulence on S_T being assumed to be basically similar to the influence of the incoming turbulence on S_T. Since that pioneering studies, flame-generated turbulence and other thermal expansion effects were in the focus of research into premixed turbulent combustion, but progress in understanding and modeling them has yet been rather moderate, as reviewed elsewhere [3-6]. Nevertheless, to the best of the present authors' knowledge, the classical concept [1,2] of combustion acceleration due to flame-generated turbulence has never been disputed, at least in the case of weak or moderate turbulence associated with a well-pronounced increase in S_T by the rms turbulent velocity u' [7].

On the one hand, this concept is indirectly supported by well-documented self-acceleration of large-scale laminar flames [8-14], which is commonly attributed to development of the flame instabilities [10-14], followed by generation of turbulence due to combustion-induced thermal expansion [8,9,15]. On the other hand, certain fundamental issues associated with that concept have not yet been resolved properly.

In particular, first, while the physical mechanisms highlighted by Karlovitz et al. [1] and by Scurlock and Grover [2] are relevant to turbulence downstream of the instantaneous flame, physical mechanisms of eventual influence of a premixed flame on the turbulent flow upstream of the flame have yet been understood poorly. However, since a flame propagates into the unburned gas, perturbations of the incoming turbulent flow are required in order for the thermal expansion effects to cause self-acceleration of the flame.

Second, combustion-induced flow perturbations may differ fundamentally from the incoming turbulence. For instance, if the flow perturbations are caused by pressure perturbations generated due to density drop in the instantaneous flame, then, the flow perturbations are expected to be irrotational (potential), whereas the rotational motion dominates in a typical constant-density turbulent flow. Indeed, certain DNS data indicate that the potential component of the gas velocity is increased (when compared to the rotational component) upstream and in vicinity of a premixed flame in a weakly turbulent flow [6].

Third, rotational perturbations generated due to thermal expansion effects in a flame, e.g., vorticity generation due to baroclinic torque [5], and turbulent eddies in the incoming flow may affect the flame surface area and, hence, burning rate in opposite directions, i.e., the former rotational perturbations may mitigate an increase in the area under the influence of the incoming turbulence. To the best of the present authors' knowledge, such a scenario has never been discussed in the turbulent combustion literature. On the contrary, the influence of flame-generated turbulence on S_T is typically assumed to be basically equivalent to the influence of the incoming turbulence on S_T, i.e., both kinds of turbulence are often considered to increase flame speed in a similar manner.

Nevertheless, there are theoretical and qualitative reasons for hypothesizing the former, commonly disregarded scenario, i.e., reduction of flame-surface area, caused by the rotational motion induced due to thermal expansion in the flame. First, the well-recognized theory of the hydrodynamic instability of a laminar premixed flame [16-19] addresses an infinitely thin flame front in a 2D potential flow of unburned reactants and yields the following expressions [5]

$$\begin{gathered}\xi(y,t)=\xi_0 \mathrm{e}^{\beta t}\cos(ky), \qquad \beta=\frac{\sigma k S_L}{1+\sigma}\left(\sqrt{1+\sigma-\sigma^{-1}}-1\right),\\ u_b=\underbrace{\sigma\xi_0\beta\,\frac{kS_L+\beta}{\sigma kS_L-\beta}\,\mathrm{e}^{\beta t-kx}\cos(ky)}_{u_{b,p}}+\underbrace{\frac{(\sigma+1)\xi_0\beta}{1-\sigma kS_L/\beta}\,\mathrm{e}^{\beta[t-x/(\sigma S_L)]}\cos(ky)}_{u_{b,r}},\\ v_b=\underbrace{\sigma\xi_0\beta\,\frac{kS_L+\beta}{\sigma kS_L-\beta}\,\mathrm{e}^{\beta t-kx}\sin(ky)}_{v_{b,p}}+\underbrace{\frac{\beta}{\sigma kS_L}\,\frac{(\sigma+1)\xi_0\beta}{1-\sigma kS_L/\beta}\,\mathrm{e}^{\beta[t-x/(\sigma S_L)]}\sin(ky)}_{v_{b,r}},\end{gathered} \tag{1}$$

where $\xi(y,t)$ is perturbation of the x-coordinate of the laminar flame front; ξ_0 is the magnitude of the initial perturbation of the front shape with respect to $\xi(y,0)=0$; $\beta>0$ and $k\ll\xi_0^{-1}$ are the perturbation growth rate and wavenumber, respectively; S_L is the laminar flame speed, $\sigma=\rho_u/\rho_b$ is the density ratio; u_b and v_b are the x and y-components of the velocity vector $\mathbf{u}_b$; and subscripts u and b designate unburned reactants and burned products, respectively. Inspection of Eq. (1) shows that (i) $\nabla\times\mathbf{u}_{b,p}=0$, (ii) $\nabla\times\mathbf{u}_{b,r}\neq 0$, (iii) $\sigma kS_L/\beta>1$, and, therefore, (iv) $\xi u_{b,r}<0$. Thus, the rotational component $u_{b,r}$ of the axial product velocity works to smooth out perturbations of the front shape, i.e., to mitigate the instability. Nevertheless, the hydrodynamic instability develops under the influence of the potential flow perturbations $\mathbf{u}_{b,p}$, which overwhelm the rotational ones. At the same time, the hydrodynamic instability and appearance of the rotational flow perturbations in the products are inextricably linked, as follows from the theory by Landau [16].

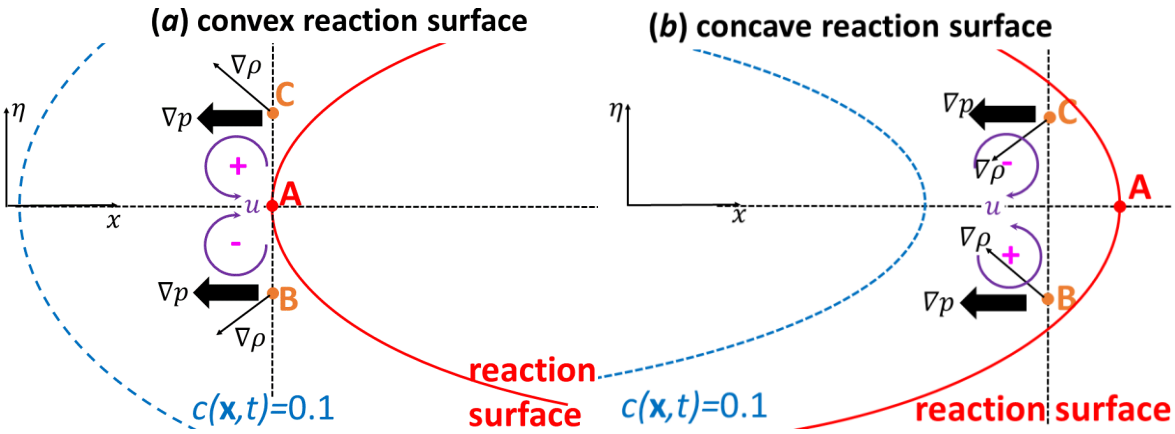

Figure 1. Generation of vorticity by baroclinic torque in the vicinity of reaction zones (a) convex or (b) concave towards unburned gas.

Second, to illustrate that flame-generated vorticity can impede growing flame surface area and burning velocity in a turbulent flow, let us consider the flow within flamelet preheat zone in the vicinity of the reaction zone convex or concave towards unburned gas, see Figs. 1a and 1b, respectively. Here, the cold boundary of the preheat zone and the reaction surface, i.e., a surface characterized by the peak reaction rate, are shown in blue dashed and red solid lines, respectively. The turbulent flame is statistically 1D, planar, normal to the x-axis, and propagates from right to left. Since baroclinic torque, i.e., vector-term $\mathbf{B_\omega} = (\nabla\rho \times \nabla p)/\rho^2$ in the transport equation for vorticity $\boldsymbol{\omega} = \nabla \times \mathbf{u}$, is the sole direct cause of vorticity generation due to thermal expansion in a premixed turbulent flame [5], let us consider behavior of a transverse ($\eta = y$ or $\eta = z$) component of this vector-term, as well as behavior of the local pressure and density gradients. Here, $\mathbf{u}$ is the velocity vector, and p is the pressure.

For simplicity, let us assume that the local pressure gradient is parallel to the x-axis, i.e., normal to the mean flame brush. Then, mutual orientation of ∇p (bold black arrows) and the projection of vector $\nabla\rho$ (see fine black arrows) on the transverse plane shown in Fig. 1a indicates that the normal (to the plane) component of the vector $\mathbf{B_\omega}$ points to (from) the reader at positive (negative) values of the local transverse coordinate η counted from the transverse coordinate of the locally leading point A, see red circle. More specifically, $B_{\omega,y} < 0$ if $\eta = z - z_A > 0$, but $B_{\omega,y} > 0$ if $\eta = z - z_A < 0$, whereas $B_{\omega,z} > 0$ if $\eta = y - y_A > 0$, but $B_{\omega,z} < 0$ if $\eta = y - y_A < 0$. Here, y_A and z_A are the y and z-coordinates of the leading point A.

Accordingly, baroclinic torque locally works to generate a vortex pair, see violet arcs, with a symmetry axis parallel to the x-axis, see horizontal dashed straight line. Moreover, by virtue of the aforementioned orientation of the normal (to the considered plane) component of $\mathbf{B_\omega}$, the axial velocity component u associated with such a vortex pair is positive in the vicinity of the symmetry axis, see violet arrows. Therefore, the local axial velocity associated with the local flame-generated vorticity pushes the leading point inside the mean flame brush, thus, reducing the reaction-surface area and, consequently, turbulent burning rate.

A similar conclusion regarding reduction of the reaction-surface area due to vorticity generated by baroclinic torque can be drawn by considering Fig. 1b, where behaviors of the vectors $\nabla\rho$, ∇p, $\mathbf{B_\omega}$, and $\boldsymbol{\omega}$ and the axial velocity u are sketched in the vicinity of a locally trailing point A on the reaction surface concave to unburned reactants.

Thus, both the theory of the hydrodynamic instability of laminar premixed flames and physical scenarios sketched in Fig. 1 imply that, contrary to the widely accepted concept of combustion acceleration due to flame-generated turbulence [1,2], flame-generated vorticity

may impede growing reaction-surface area, thus, reducing turbulent burning rate. The major goal of the present work is to examine this hypothesis, which has yet been beyond the focus of the mainstream research into flame-turbulence interaction.

To fill this gap, Direct Numerical Simulation (DNS) data generated by two of the present authors [20,21] more than 15 years ago will be analyzed. The choice of this DNS database, which may appear to be outdated when compared to recent DNS data [22-30] generated in the case of complex combustion chemistry and a high ratio of the rms turbulent velocity u' to the laminar flame speed S_L, requires comments.

Since the focus of the following discussion is placed on the influence of combustion-induced thermal expansion on the velocity, pressure, vorticity, and enstrophy fields upstream of reaction zones, detailed description of complex combustion chemistry within such zones appears to be of secondary importance when compared to two other major requirements. First, in order to make the studied thermal expansion effects as strong as possible, heat release and density drop should be localized to sufficiently thin zones and the velocity jumps across such zones should be sufficiently large when compared to the rms turbulent velocity u'. In other words, the flamelet regime [31-33] of premixed turbulent combustion associated with a low u'/S_L should be addressed. The selected DNS data are indeed associated with this regime, as discussed in details elsewhere [34], whereas the vast majority of recent very advanced DNS studies attacked other combustion regimes characterized by a large u'/S_L.

Second, to better explore the thermal expansion effects, data obtained at significantly different density ratios σ are required. The selected DNS database does satisfy this requirement, because cases of $\sigma = 2.5$ and 7.53 were simulated, with all other things being roughly equal. As discussed in details elsewhere [35], such variations in the density ratio offer an opportunity to explore two opposite scenarios, which are directly relevant to the major goal of the present study. These are; (i) generation of vorticity due to baroclinic torque overwhelms dissipation of vorticity due to dilatation and viscous forces, thus, increasing enstrophy within the flame brush at $\sigma = 7.53$, but (ii) the dilatation and dissipation effects dominate and reduce enstrophy within the flame brush at $\sigma = 2.5$. Therefore, the selected DNS data appear to be fully adequate to the major goal of the present work.

Direct Numerical Simulations

Since the DNS data were discussed in details elsewhere [20,21] and were already used by various research groups [34-52], let us restrict ourselves to a very brief summary of those compressible 3D simulations. They dealt with statistically 1D and planar, equidiffusive, adiabatic flames modeled by unsteady continuity, Navier-Stokes, and energy equations, supplemented with the ideal gas state equation and a transport equation for the mass fraction Y of a deficient reactant. Temperature-dependence of molecular transport coefficients was taken into account, e.g., the kinematic viscosity $\nu = \nu_u(T/T_u)^{0.7}$, where T is the temperature. The Lewis Le and Prandtl Pr numbers were equal to 1.0 and 0.7, respectively. Combustion chemistry was reduced to a single reaction. Therefore, the mixture state was characterized with a single combustion progress variable $c = (T - T_u)/(T_b - T_u) = 1 - Y/Y_u$.

The computational domain was a rectangular box $\Lambda_x \times \Lambda_y \times \Lambda_z$, where $\Lambda_x = 8$ mm and $\Lambda_y = \Lambda_z = 4$ mm. It was resolved using a uniform rectangular ($2\Delta x = \Delta y = \Delta z$) mesh of $512 \times 128 \times 128$ points. The flow was periodic in y and z directions.

Using an energy spectrum $E(\kappa)$ proposed by Kraichnan [53], homogeneous isotropic turbulence was generated [20] in a separate box and was injected into the computational domain through the left boundary $x = 0$. The generated turbulence was characterized [20] by $u' = 0.53$ m/s and an integral length scale $L = 3.45$ mm. Accordingly, the turbulent Reynolds number $Re_t = u'L/\nu_u = 96$.

At $t = 0$, a planar laminar flame was embedded into statistically the same turbulence assigned for the velocity field in the entire computational domain. Subsequently, the mean inflow velocity U was increased twice, $U(0 \le t < t_1) = S_L < U(t_1 \le t < t_2) < U(t_2 \le t)$, with $U(t_2 \le t)$ being close to the mean turbulent flame speed $\overline{S_T(t_2 \le t \le t_3)}$ in order to keep the flame in the computational domain till the end t_3 of the simulations.

Three DNS data sets H, M, and L associated with High, Medium, and Low, respectively, density ratios σ were originally generated [20,21]. Since the focus of the present study is placed on thermal expansion effects, the following discussion will be restricted to results obtained in two cases characterized by the highest and the lowest density ratios, i.e., flame H ($\sigma = 7.53$, $S_L = 0.6$ m/s, $\delta_L = 0.217$ mm) and flame L ($\sigma = 2.5$, $S_L = 0.416$ m/s, $\delta_L = 0.158$ mm). In both cases, $\overline{S_T(t_2 \le t \le t_3)}/S_L = 1.9$. Here, $\delta_L = (T_b - T_u)/\max\{|\nabla T|\}$ is the laminar flame thickness. The two flames are well associated with the flamelet combustion regime, e.g., various Bray-Moss-Libby (BML) expressions hold in cases H and L, see figures 1-4 in Ref. [34].

Since turbulence decays along the direction x of the mean flow, the turbulence characteristics are slightly different at the leading edges of the H and L-flame brushes, e.g., $u' = 0.33$ m/s, $\lambda = 0.43$ mm, $\eta = 0.075$ mm, $Da = 17.5$, and $Ka = 0.06$ in case H or $u' = 0.38$ m/s, $\lambda = 0.47$ mm, $\eta = 0.084$ mm, $Da = 10.0$, and $Ka = 0.10$ in case L. Here, $Da = \tau_T/\tau_f$ and $Ka = \tau_f u'/\lambda$ are the Damköhler and Karlovitz numbers, respectively, $\tau_f = \nu_u/(PrS_L^2)$ and $\tau_T = \bar{k}^{3/2}/\bar{\varepsilon}$ are flame and turbulence time scales, respectively, $\lambda = u'/\sqrt{15\,\nu/\bar{\varepsilon}}$ and $\eta = (\nu^3/\bar{\varepsilon})^{1/4}$ are the Taylor and Kolmogorov length scales, respectively, $k = \left(u_j u_j - \bar{u}_j \bar{u}_j\right)/2$ and $\varepsilon = 2\nu S_{ij} S_{ij}$ are the turbulent kinetic energy and its dissipation rate, respectively, $u' = \left(2\bar{k}/3\right)^{1/2}$ is the rms turbulent velocity, $S_{ij} = 0.5\left(\partial u_i/\partial x_j + \partial u_j/\partial x_i\right)$ is the rate-of-strain tensor, and the summation convention applies for repeated indexes.

The DNS data were processed as follows. Mean quantities $\bar{q} = \bar{q}(x)$ were averaged over a transverse plane of x =const and over time (221 and 200 snapshots in cases H and L, respectively, stored during a time interval of $t_3 - t_2 \approx 1.5\,L/u_0' \approx 10$ ms). Subsequently, x-dependencies were mapped to $\bar{c}$-dependencies using the spatial profiles of the Reynolds-averaged combustion progress variable $\bar{c}(x)$.

Results and Discussion

Since the rate of an increase (or decrease) in the local area A^* of an iso-scalar surface $c(\mathbf{x}, t) = c^*$is well known to be controlled by the local stretch rate $\dot{s} = \nabla \cdot \mathbf{u} - \mathbf{nn}: \boldsymbol{\nabla}\mathbf{u} + S_d \nabla \cdot \mathbf{n}$ [17,54-56], i.e., $d\ln A^*/dt = \dot{s}$, the focus of the following discussion will be placed on the joint statistics of $\dot{s}$ and enstrophy $\Omega = \boldsymbol{\omega} \cdot \boldsymbol{\omega}$ or baroclinic torque term $B_\Omega = \boldsymbol{\omega} \cdot \mathbf{B}_{\boldsymbol{\omega}}$ in the transport equation for the enstrophy [35]. Here, $\mathbf{n} = -\nabla c/|\nabla c|$ is the unit vector normal to the iso-scalar surface, $S_d = [\nabla \cdot (\rho D \nabla c) + W]/(\rho|\nabla c|)$ is the local displacement speed, D is the molecular diffusivity of c, and W is the mass rate of product creation.

Figure 2 shows that the probability of negative (black solid lines) stretch rates is higher than the probability of $\dot{s}(\mathbf{x}, t) > 0$ (red dashed lines) in regions characterized by a large magnitude of $B_\Omega(\mathbf{x}, t)$. On the contrary, relation between the two computed probabilities is well known to be opposite if they are extracted from the entire flame brush and the present DNS data also show this, e.g. see Fig. 5b discussed later. Since the rate $d\ln A^*/dt$ of an increase or decrease in the logarithm of an infinitesimal area A^* of a propagating surface is equal to the local stretch rate [17,54-56], Fig. 2 indicates that the area of a surface of $c(\mathbf{x}, t) = c^*$ is statistically reduced in regions associated with the strongest generation of enstrophy due to baroclinic torque.

Such a trend is not observed within flamelet preheat zone ($c < 0.65$), where the local stretch rates are predominantly positive, e.g., see Fig. 3a, but is well pronounced in the vicinity of the reaction zone ($c > 0.65$), where $\dot{s}(\mathbf{x}, t)$ is predominantly negative provided that $B_\Omega(\mathbf{x}, t)$ is

sufficiently large, e.g., see Fig. 3b. Even at the reaction zone, the trend is not pronounced at the leading edge of the mean flame brush, e.g., see Fig. 4a, but is well pronounced in the middle of the flame brush, e.g., see Fig. 4b, or at larger $\bar{c}(x)$.

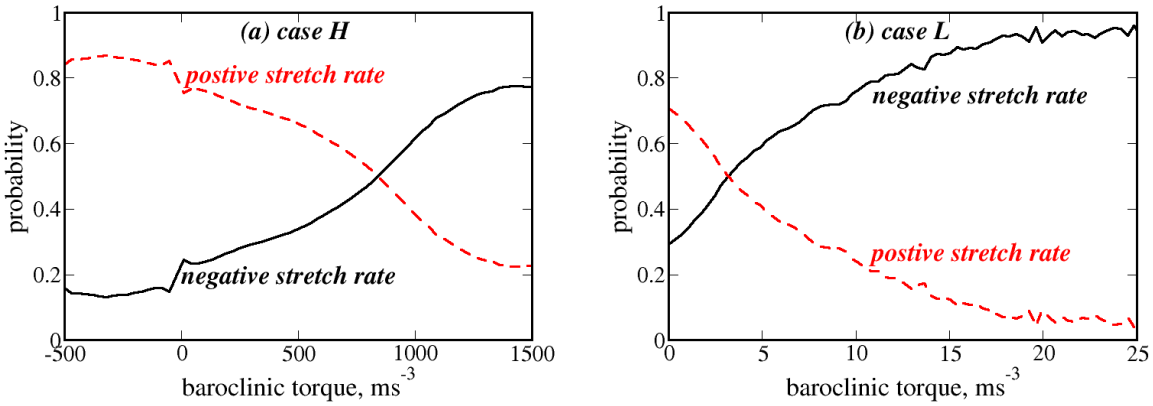

Figure 2. Probabilities of positive (red dashed lines) and negative (black solid lines) stretch rates conditioned on the local value of baroclinic torque term $B_\Omega(\mathbf{x},t)$ in the transport equation for enstrophy. (a) case H, (b) case L.

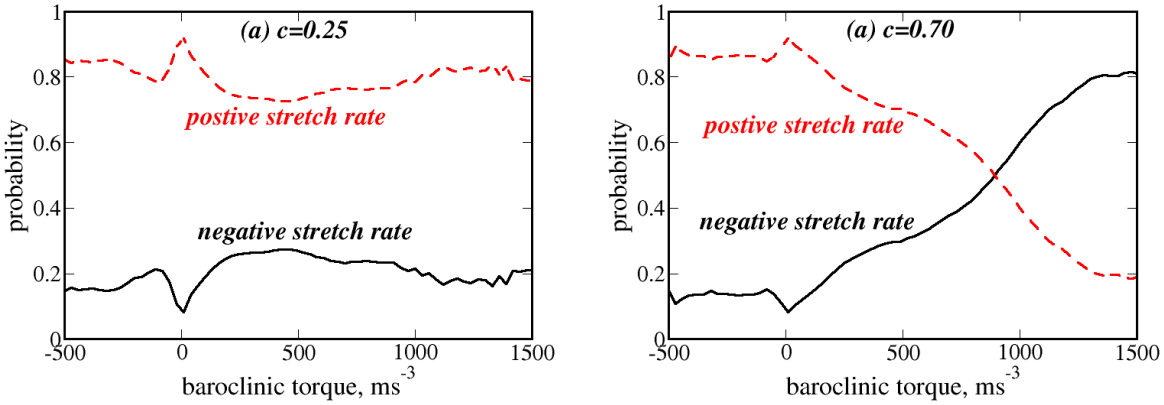

Figure 3. Probabilities of positive (red dashed lines) and negative (black solid lines) stretch rates doubly conditioned on (i) the local value of baroclinic torque term $B_\Omega(\mathbf{x},t)$ in the transport equation for enstrophy and (ii) the local value of the combustion progress variable. (a) $0.20 < c(\mathbf{x},t) < 0.30$, (b) $0.65 < c(\mathbf{x},t) < 0.75$. Case H.

Thus, the discussed reduction effect of baroclinic torque on the rate $d\ln A^*/dt$ is enhanced both by c^* and $\bar{c}(x)$. The former trend may be attributed to shortage of time during that baroclinic torque has affected fluid particles that reach an iso-scalar surface characterized by a low c^*. The latter trend may be attributed to an increase in the magnitude of $B_\Omega(\mathbf{x},t)$ with increasing $\bar{c}(x)$, e.g., cf. abscissa coordinates in Figs. 4a and 4b.

Figure 5a shows that, in case H, the probability of negative (black solid line) stretch rates is higher than the probability of $\dot{s}(\mathbf{x},t) > 0$ (red dotted-dashed lines) in regions characterized by a large enstrophy $\Omega(\mathbf{x},t)$. A similar trend was already discussed for regions characterized by a large magnitude of baroclinic torque term $B_\Omega(\mathbf{x},t)$. However, in case L, results plotted in Fig. 5b differ qualitatively from results shown in Fig. 2b, i.e., stretch rates are predominately positive independently on $\Omega(\mathbf{x},t)$. This difference between results plotted in Figs. 2b and 5b is

associated with the fact that the magnitude of $B_\Omega(\mathbf{x},t)$ is much less in case L when compared to case H, cf. abscissas in Figs. 2a and 2b. Accordingly, baroclinic torque barely affects the vorticity field in case L and the enstrophy decays within the mean flame brush [35]. Thus, flame-generated vorticity is weak and plays a minor role in case L.

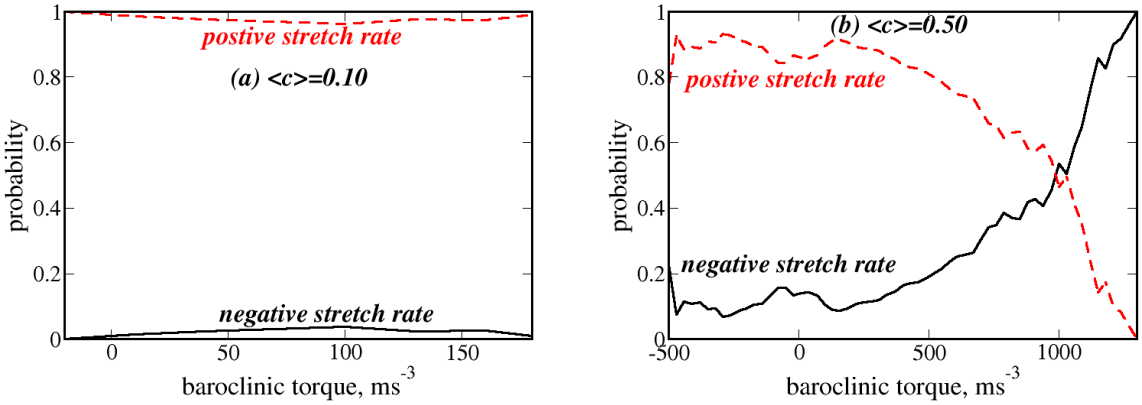

Figure 4. Probabilities of positive (red dashed lines) and negative (black solid lines) stretch rates doubly conditioned on (i) the local value of baroclinic torque term $B_\Omega(\mathbf{x},t)$ in the transport equation for enstrophy and (ii) the local value of the combustion progress variable $0.65 < c(\mathbf{x},t) < 0.75$. The probabilities are evaluated in two different regions of the mean flame brush. (a) $0.05 < \bar{c}(x) < 0.15$, (b) $0.45 < \bar{c}(x) < 0.55$. Case H.

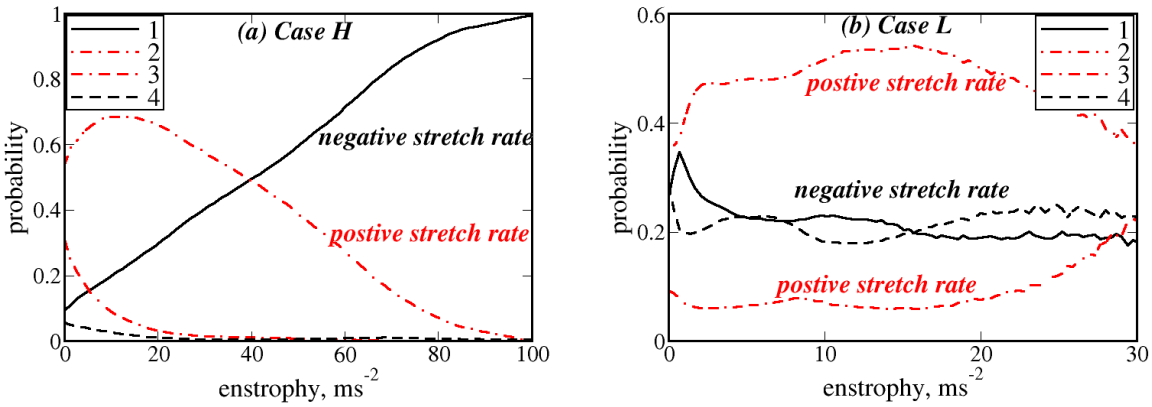

Figure 5. Probabilities of positive (red dashed lines 2 and 3) and negative (black solid lines 1 and 4) stretch rates conditioned on the local value of enstrophy $\Omega(\mathbf{x},t)$. Curves 1-2 and 3-4 are associated with the positive and negative, respectively, baroclinic torque term $B_\Omega(\mathbf{x},t)$. (a) case H, (b) case L.

To evaluate the contribution of regions characterized by a large magnitude of $B_\Omega(\mathbf{x},t)$ or $\Omega(\mathbf{x},t)$ to the evolution of the local areas of various iso-scalar surfaces $c(\mathbf{x},t) = c^*$, the mean rate of an increase in the surface area, conditioned on $c_1 < c(\mathbf{x},t) < c_2$ and $Q_1 < Q(\mathbf{x},t) < Q_2$, was calculated as follows

$$\left\langle \frac{d\Sigma}{dt} \middle| c_1 < c < c_2 \middle| Q_1 < Q < Q_2 \right\rangle = \frac{\int_{t_2}^{t_3} \iiint \dot{s}|\nabla c| \Pi(c_1<c<c_2)\Pi(Q_1<Q<Q_2) d\mathbf{x}dt}{\int_{t_2}^{t_3} \iiint \Pi(c_1<c<c_2)\Pi(Q_1<Q<Q_2) d\mathbf{x}dt}. \quad (2)$$

Here, Q designates either the baroclinic torque term B_Ω or enstropy Ω, the difference $\Pi(q_1 < q < q_2) \equiv H(q - q_2) - H(q - q_1)$ between Heaviside functions $H(q)$ is equal to unity if an arbitrary quantity q satisfies the following constraint $q_1 < q < q_2$, but $H(q)$ vanishes otherwise, $\Sigma = |\nabla c|$ is flame surface density, and the integral in the numerator characterizes the rate of an increase in the surface area, because, for an infinitesimal volume dV, the local area $\delta A^* = \Sigma^* dV$ and $d(\delta A^*)/dt = \dot{s}\delta A^* = \dot{s}|\nabla c|_{c=c^*} dV$.

Figures 6a and 7a show that, both in the reaction zone (see red solid lines) and in the middle of flamelets (orange dotted-dashed lines) in case H, the doubly conditioned rate given by Eq. (2) is negative in regions characterized by either a large $B_\Omega(\mathbf{x}, t)$ or a large $\Omega(\mathbf{x}, t)$, respectively. Thus, Figs. 6a and 7a further support the finding that generation of vorticity due to baroclinic torque within flame can work to impede increasing the flame-surface area.

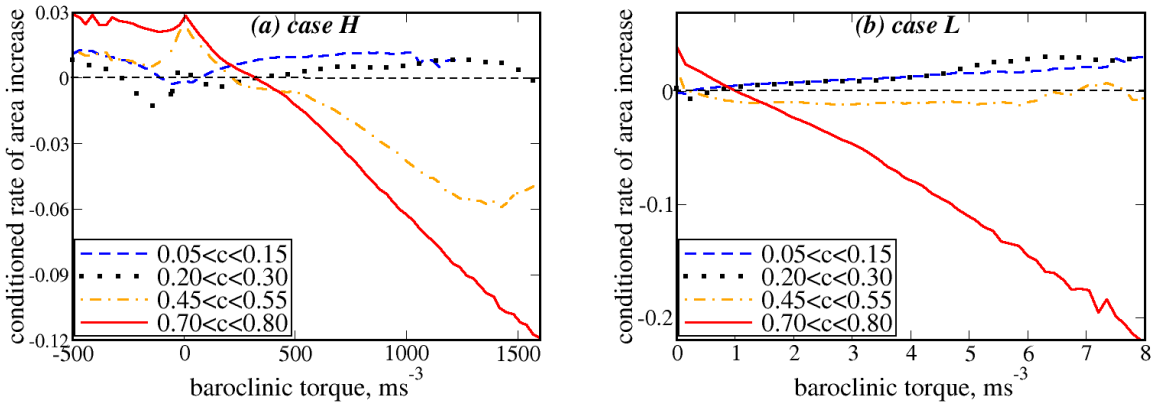

Figure 6. Doubly conditioned rate of an increase in flame surface area, given by Eq. (2) and normalized using D_u/S_L^3, vs. baroclinic torque term B_Ω in the enstrophy transport equation. Intervals $c_1 < c(\mathbf{x}, t) < c_2$ that the rate is conditioned to are specified in the legends. (a) case H, (b) case L.

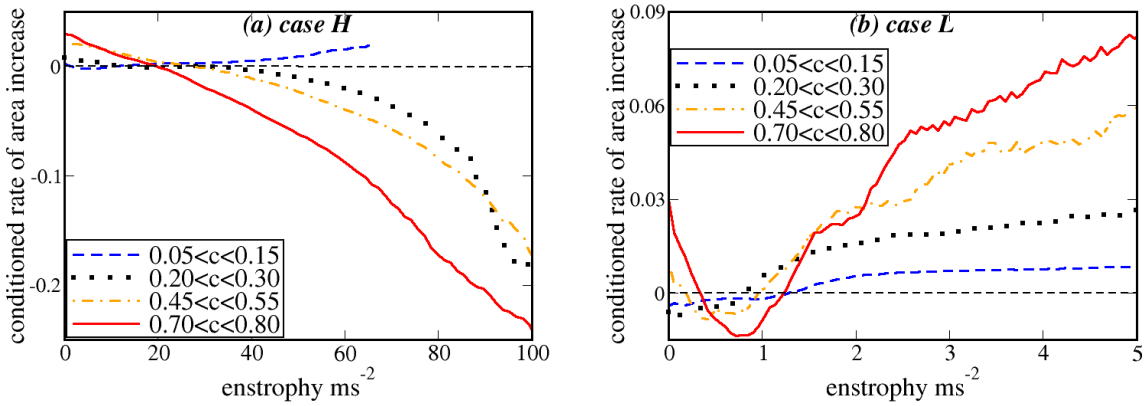

Figure 7. Doubly conditioned rate of an increase in flame surface area, given by Eq. (2) and normalized using D_u/S_L^3, vs. enstrophy Ω. Intervals $c_1 < c(\mathbf{x}, t) < c_2$ that the rate is conditioned to are specified in the legends. (a) case H, (b) case L.

The same trend is observed for the reaction zone and the largest $B_\Omega(\mathbf{x}, t)$ in case L, see red solid line in Fig. 6b, but the discussed rate is positive in regions characterized by the largest enstrophy $\Omega(\mathbf{x}, t)$, see Fig. 7b. As already discussed above, the latter trend is associated with a

weak influence of baroclinic torque on enstrophy evolution in case L, in which positive stretch rates dominate independently of $\Omega(\mathbf{x},t)$ similarly to constant-density turbulent flows.

Furthermore, a relative mean bulk rate of an increase in the surface area in volumes characterized by $Q_1 < Q(\mathbf{x},t) < Q_2$ when compared to the entire flame brush was evaluated as follows

$$\langle \delta A | c_1 < c < c_2 | Q_1 < Q < Q_2 \rangle = \frac{\int_{t_2}^{t_3} \iiint \dot{s} |\nabla c| \Pi(c_1<c<c_2) \Pi(Q_1<Q<Q_2) d\mathbf{x} dt}{\int_{t_2}^{t_3} \iiint \dot{s} |\nabla c| \Pi(c_1<c<c_2) d\mathbf{x} dt}. \quad (3)$$

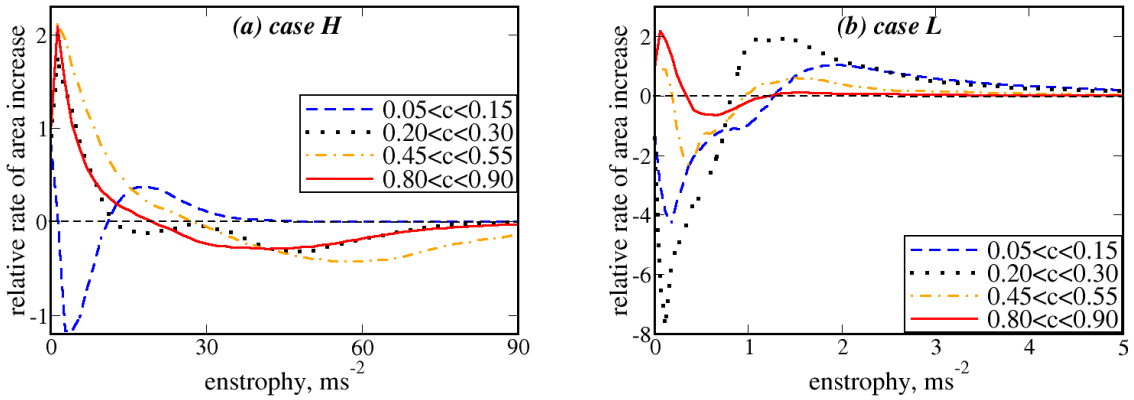

Figure 8. Doubly conditioned relative mean bulk rate of an increase in flame surface area, given by Eq. (3), vs. enstrophy Ω. Intervals $c_1 < c(\mathbf{x},t) < c_2$ that the rate is conditioned to are specified in the legends. (a) case H, (b) case L.

Figure 8a shows that, both in the reaction zone (see red solid lines) and in the middle of flamelets (orange dotted-dashed lines) in case H, the relative mean bulk rate given by Eq. (3) is negative in regions characterized by a large $\Omega(\mathbf{x},t)$, with the magnitude of this negative rate being significant. Thus, reduction of reaction-surface area (see red solid lines) by flame-generated vorticity plays a substantial role in case H. On the contrary, in case L characterized by a low density ratio, this physical mechanism is of minor importance, see Fig. 8b. Even if the relative mean bulk rate conditioned on the reaction zone is negative in regions characterized by a large $B_\Omega(\mathbf{x},t)$ in case L (not shown), the magnitude of this rate is very low due to a weak influence of baroclinic torque on enstrophy in case L, as already discussed earlier.

Conclusions

DNS data analyzed in the present paper indicate that vorticity generation by baroclinic torque can impede increasing the area of reaction-zone surface, contrary to the common concept of combustion acceleration due to flame-generated turbulence. Such an effect is more pronounced at larger values of the mean combustion progress variable $\bar{c}$ and at larger density ratios. If the density ratio is low, e.g., $\sigma = 2.5$, baroclinic torque weakly effects vorticity field within mean flame brush and the aforementioned effect is not observed.

It is worth stressing that the present work does not aim at claiming that the influence of combustion-induced thermal expansion on turbulence reduces the reaction-surface area and, hence, burning rate. The potential velocity perturbations can overwhelm the rotational perturbations and can result in increasing burning rate, as occurs in the case of a hydrodynamically unstable laminar premixed flame [16]. For instance, unburned mixture

fingers discussed in details elsewhere [42,48] evidence an increase in flame surface area and turbulent burning rate due to combustion-induced thermal expansion.

However, if turbulence is considered to be inherently rotational flow, then, the influence of flame-generated turbulence on burning rate appears to be fundamentally different from the influence of turbulence in the incoming reactants on the rate. Accordingly, the concept of combustion acceleration due to flame-generated turbulence should be revisited and models developed for predicting an increase in burning rate by vorticity in the incoming turbulent flow are unlikely to be useful for describing a decrease in reaction-surface area and, hence, burning rate due to flame-generated vorticity. In other words, the influence of the incoming turbulence on burning rate should clearly be distinguished from the influence of flame-generated vorticity on the rate and the two effects can be opposite.

Acknowledgements

ANL gratefully acknowledges the financial support by the Chalmers Transport and Energy Areas of Advance, and by the Combustion Engine Research Center. VAS gratefully acknowledges the financial support by ONERA and by the Grant of the Ministry of Education and Science of the Russian Federation (Contract No. 14.G39.31.0001 of 13.02.2017).

References

[1] Karlovitz, B., Denniston, D.W., Wells, F.E., "Investigation of turbulent flames", *J. Chem. Phys.* 19:541-547 (1951).

[2] Scurlock, A.C., Grover, J.H., "Propagation of turbulent flames", *Proc. Combust. Inst.* 4:645-658 (1953).

[3] Günther, R., "Turbulence properties of flames and their measurement", *Prog. Energy Combust. Sci.* 9:105-154 (1983).

[4] Bray, K.N.C., "Turbulent transport in flames", *Proc. R. Soc. London A* 451:231-256 (1995).

[5] Lipatnikov, A.N., Chomiak, J., "Effects of premixed flames on turbulence and turbulent scalar transport", *Prog. Energy Combust. Sci*. 36:1-102 (2010).

[6] Sabelnikov, V.A., Lipatnikov, A.N., "Recent advances in understanding of thermal expansion effects in premixed turbulent flames", *Annu. Rev. Fluid Mech.* 49:91-117 (2017).

[7] Lipatnikov, A.N., Chomiak, J., "Turbulent burning velocity and speed of developing, curved, and strained flames", *Prog. Energy Combust. Sci.* 28:1-74 (2002).

[8] Gostintsev, Y.A., Istratov, A.G., Shulenin, Y.V., "Self-similar propagation of a free turbulent flame in mixed gas mixtures", *Combust. Explos. Shock Waves* 24:563-568 (1988).

[9] Gostintsev, Y.A., Istratov, A.G., Kidin, N.I., Fortov, V.E., "Self-turbulization of gas flames: An analysis of experimental results", *High Temperature* 37(2):282-288 (1999).

[10] Bradley, D., "Instabilities and flame speeds in large-scale premixed gaseous explosions", *Phil. Trans. R. Soc. London* 357:3567-3581 (1999).

[11] Addabbo, R., Bechtold, J.K., Matalon, M., "Wrinkling of spherically expanding flames", *Proc. Combust. Inst.* 29:1527-1535 (2002).

[12] Sivashinsky, G.I., "Some developments in premixed combustion modeling", *Proc. Combust. Inst.* 29:1737-1761 (2002).

[13] Matalon, M., "Flame dynamics", *Proc. Combust. Inst.* 32:57-82 (2009).

[14] Akkerman, V., Law, C.K., Bychkov, V., "Self-similar accelerative propagation of expanding wrinkled flames and explosion triggering", *Phys. Rev. E* 83:026305 (2011).

[15] Kerstein, A.R., "Turbulence in combustion processes: modeling challenges", *Proc. Combust. Inst.* 29:1763-1773 (2002).

[16] Landau, L.D., "On the theory of slow combustion", *Acta Psysicochimica USSR* 19:77-85 (1944).
[17] Zel'dovich, Ya.B., Barenblatt, G.I., Librovich, V.B., Makhviladze, G.M., *The Mathematical Theory of Combustion and Explosions*, Consultants Bureau, 1985.
[18] Clavin, P., "Dynamical behavior of premixed flame fronts in laminar and turbulent flows", *Prog. Energy Combust. Sci*. 11:1-59 (1985).
[19] Matalon, M., "Intrinsic flame instabilities in premixed and nonpremixed combustion", *Annu. Rev. Fluid Mech.* 39:163-191 (2007).
[20] Nishiki, S., Hasegawa, T., Borghi, R., Himeno, R., "Modeling of flame-generated turbulence based on direct numerical simulation databases", *Proc. Combust. Inst.* 29:2017-2022 (2002).
[21] Nishiki, S., Hasegawa, T., Borghi, R., Himeno, R., "Modelling of turbulent scalar flux in turbulent premixed flames based on DNS databases", *Combust. Theory Modell*. 10:39-55 (2006).
[22] Carlsson, H., Yu, R., Bai, X.-S., "Flame structure analysis for categorization of lean premixed CH_4/air and H_2/air flames at high Karlovitz numbers: Direct numerical simulation studies", *Proc. Combust. Inst.* 35:1425-1432 (2015).
[23] Uranakara, H.A., Chaudhuri, S., Dave, H.L., Arias, P.G., Im, H.G., "A flame particle tracking analysis of turbulence-chemistry interaction in hydrogen-air premixed flames", *Combust. Flame* 163:220-240 (2016).
[24] Aspden, A.J., Day, M.J., Bell, J.B., "Three-dimensional direct numerical simulation of turbulent lean premixed methane combustion with detailed kinetics", *Combust. Flame* 165:266-283 (2016).
[25] Cecere, D., Giacomazzi, E., Arcidiacono, N.M., Picchia, F.R., "Direct numerical simulation of a turbulent lean premixed CH_4/H_2-air slot flame", *Combust. Flame* 165:384-401 (2016).
[26] Bobbitt, B., Lapointe, S., Blanquart, G., "Vorticity transformation in high Karlovitz number premixed flames", *Phys. Fluids* 28:015101 (2016).
[27] Wang, H., Hawkes, E.R., Zhou, B., Chen, J.H., Li, Z., Aldén, M., "A comparison between direct numerical simulation and experiment of the turbulent burning velocity-related statistics in a turbulent methane-air premixed jet flame at high Karlovitz number", *Proc. Combust. Inst.* 36:2045-2053 (2017).
[28] Chaudhuri, S., Kolla, H., Dave, H.L., Hawkes, E.R., Chen, J.H., Law, C.K., "Flame thickness and conditional scalar dissipation rate in a premixed temporal turbulent reacting jet", *Combust. Flame* 184:273-285 (2017).
[29] MacArt, J.F., Grenga, T., Mueller, M.E., "Effects of combustion heat release on velocity and scalar statistics in turbulent premixed jet flames at low and high Karlovitz numbers", *Combust. Flame* 191:468-485 (2018).
[30] Minamoto, Y., Yenerdag, B., Tanahashi, M., "Morphology and structure of hydrogen-air turbulent premixed flames", *Combust. Flame* 192:369-383 (2018).
[31] Borghi, R., "On the structure and morphology of turbulent premixed flames", *Recent Advances in Aerospace Science*, Eds. by Casci, S., Bruno, C., Plenum, 1984, pp. 117-138.
[32] Williams, F.A., *Combustion Theory*, 2nd ed., Benjamin/Cummings, 1985, p. 412.
[33] Peters, N., *Turbulent Combustion*, Cambridge University Press, 2000.
[34] Lipatnikov, A.N., Nishiki, S., Hasegawa, T., "DNS assessment of relation between mean reaction and scalar dissipation rates in the flamelet regime of premixed turbulent combustion", *Combust. Theory Modell*. 19:309-328 (2015).
[35] Lipatnikov, A.N., Nishiki, S., Hasegawa, T., "A direct numerical simulation study of vorticity transformation in weakly turbulent premixed flames", *Phys. Fluids* 26:105104 (2014).

[36] Im, Y.H., Huh, K.Y., Nishiki, S., Hasegawa, T., "Zone conditional assessment of flame-generated turbulence with DNS database of a turbulent premixed flame", *Combust. Flame* 137:478-488 (2004).
[37] Mura, A., Tsuboi, K., Hasegawa, T., "Modelling of the correlation between velocity and reactive scalar gradients in turbulent premixed flames based on DNS data", *Combust. Theory Modell*. 12:671-698 (2008).
[38] Mura, A., Robin, V., Champion, M., Hasegawa, T., "Small scale features of velocity and scalar fields in turbulent premixed flames", *Flow Turbul. Combust*. 82:339-358 (2009).
[39] Robin, V., Mura, A., Champion, M., Hasegawa, T., "Direct and indirect thermal expansion effects in turbulent premixed flames", *Combust. Sci. and Tech*. 182:449-464 (2010).
[40] Robin, V., Mura, A., Champion, M., "Modeling of the effects of thermal expansion on scalar turbulent fluxes in turbulent premixed flames", *J. Fluid Mech*. 689:149-182 (2011).
[41] Bray, K.N.C., Champion, M., Libby, P.A., Swaminathan, N., "Scalar dissipation and mean reaction rates in premixed turbulent combustion", *Combust. Flame* 158:2017-2022 (2011)
[42] Lipatnikov, A.N., Chomiak, J., Sabelnikov, V.A., Nishiki, S., Hasegawa, T., "Unburned mixture fingers in premixed turbulent flames", *Proc. Combust. Inst.* 35:1401-1408 (2015).
[43] Lipatnikov, A.N., Sabelnikov, V.A., Nishiki, S., Hasegawa, T., Chakraborty, N., "DNS assessment of a simple model for evaluating velocity conditioned to unburned gas in premixed turbulent flames", *Flow Turbul. Combust.* 94:513-526 (2015).
[44] Sabelnikov, V.A., Lipatnikov, A.N., Chakraborty, N., Nishiki, S., Hasegawa, T., "A transport equation for reaction rate in turbulent flows", *Phys. Fluids* 28:081701 (2016).
[45] Sabelnikov, V.A., Lipatnikov, A.N., Chakraborty, N., Nishiki, S., Hasegawa, T., "A balance equation for the mean rate of product creation in premixed turbulent flames", *Proc. Combust. Inst*. 36:1893-1901 (2017).
[46] Lipatnikov, A.N., Sabelnikov, V.A., Nishiki, S., Hasegawa, T., "Flamelet perturbations and flame surface density transport in weakly turbulent premixed combustion", *Combust. Theory Modell.* 21:205-227 (2017).
[47] Lipatnikov, A.N., Sabelnikov, V.A., Chakraborty, N., Nishiki, S., Hasegawa, T., "A DNS study of closure relations for convection flux term in transport equation for mean reaction rate in turbulent flow", *Flow Turbul. Combust*. 100:75-92 (2018).
[48] Lipatnikov, A.N., Chomiak, J., Sabelnikov, V.A., Nishiki, S., Hasegawa, T., "A DNS study of the physical mechanisms associated with density ratio influence on turbulent burning velocity in premixed flames", *Combust. Theory Modell*. 22:131-155 (2018).
[49] Lipatnikov, A.N., Sabelnikov, V.A., Nishiki, S., Hasegawa, T., "Combustion-induced local shear layers within premixed flamelets in weakly turbulent flows", *Phys. Fluids* 30:085101 (2018).
[50] Lipatnikov, A.N., Sabelnikov, V.A., Nishiki, S., Hasegawa, T., "Does flame-generated vorticity increase turbulent burning velocity?" *Phys. Fluids* 30:081702 (2018).
[51] Sabelnikov, V.A., Lipatnikov, A.N., Nishiki, S., Hasegawa, T., "Application of conditioned structure functions to exploring influence of premixed combustion on two-point turbulence statistics", *Proc. Combust. Inst.* 37, in press.
[52] Lipatnikov, A.N., Nishiki, S., Hasegawa, T., "A DNS assessment of linear relations between filtered reaction rate, flame surface density, and scalar dissipation rate in a weakly turbulent premixed flame", *Combust. Theory Modell.* 23, in press.
[53] Kraichnan, R.H., "Decay of isotropic turbulence in the direct-interaction approximation", *Phys. Fluids* 7:1030-1048 (1964).
[54] Matalon, M., "On flame stretch", *Combust. Sci. and Tech.* 31:169-182 (1983).
[55] Pope, S.B., "The evolution of surface in turbulence", *Int. J. Engng Sci*. 26:445-469 (1988).
[56] Candel, S., Poinsot, T., "Flame stretch and the balance equation for the flame area", *Combust. Sci. and Tech*. 170:1-15 (1990).